

LACoOT: LAYER COLLAPSE THROUGH OPTIMAL TRANSPORT

A PREPRINT

Victor Quétu, Nour Hezbri, Enzo Tartaglione
 LTCI, Télécom Paris, Institut Polytechnique de Paris, France
 {name.surname}@telecom-paris.fr

ABSTRACT

Although deep neural networks are well-known for their remarkable performance in tackling complex tasks, their hunger for computational resources remains a significant hurdle, posing energy-consumption issues and restricting their deployment on resource-constrained devices, which stalls their widespread adoption.

In this paper, we present an optimal transport method to reduce the depth of over-parametrized deep neural networks, alleviating their computational burden. More specifically, we propose a new regularization strategy based on the Max-Sliced Wasserstein distance to minimize the distance between the intermediate feature distributions in the neural network. We show that minimizing this distance enables the complete removal of intermediate layers in the network, with almost no performance loss and without requiring any finetuning. We assess the effectiveness of our method on traditional image classification setups. We commit to releasing the source code upon acceptance of the article.

Keywords Regularization · Compression · Optimal Transport · Deep-Learning

1 Introduction

The advent of deep learning has significantly improved the modeling and recognition of complex patterns for various tasks by combining non-linear functions to enhance their expressivity [Liang and Srikant, 2016, Ali Mehmeti-Göpel and Disselhoff, 2023]. Recent innovations, such as batch normalization [Ioffe and Szegedy, 2015, Santurkar et al., 2018] and residual connections [He et al., 2015], have especially enabled the training of more and more overparameterized deep neural networks (DNNs).

However, despite their enhanced performance, these networks impose substantial computational burdens due to their immense parameter counts and associated floating-point operations, hindering their deployment on edge devices and real-time applications. To alleviate these resource demands, compression techniques have emerged as essential counterbalancing strategies. Traditional parameter pruning methods [Han et al., 2015a, He and Xiao, 2023, Tartaglione et al., 2022] for instance, can achieve high sparsity levels of the DNN, but they are often suboptimal, failing to effectively reduce the network size. Therefore, efforts to specifically mitigate the depth of DNN while maintaining performance have gained traction, with approaches such as structured layer pruning [Quétu et al., 2024] and neural architecture search (NAS) [Baymurzina et al., 2022] being pursued. These methods are computationally challenging though, as they either require retraining (this involves the structured pruning approaches) or necessitate the search of the state space (for NAS).

In principle, this goal is largely achievable since DNN has been shown to exhibit high redundancy levels [Yang et al., 2024, Gromov et al., 2024] or to learn irrelevant patterns in the data, leading to the identification of layers and blocks

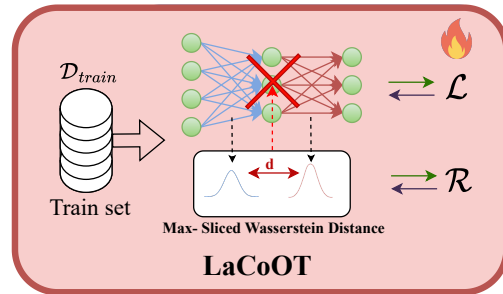


Figure 1: LaCoOT reduces neural network depth by minimizing the Max-Sliced Wasserstein distance between intermediate feature distributions.

that contribute minimally to the output. This phenomenon is further supported by the collapse phenomenon in neural networks, which has been observed at both the neuron [Zhu et al., 2021] and layer levels [Gromov et al., 2024], as well as by the shortcut learning line of study [Hermann et al., 2024]. Most existing methods do not allow for direct pruning of these redundant fragments without significant loss of performance though. Besides, they often require to fix the number of layers to be pruned a priori. Hence, formalizing the redundancy quantification metric in DNNs to strategically optimize them is still an active field of research.

This is where Optimal Transport (OT), a mathematical framework with deep historical roots [Villani, 2009, Peyré and Cuturi, 2018], comes to hand as it offers an interesting toolbox for probability distribution discrepancy quantification. More broadly, incorporating OT into depth reduction strategies seems to be a promising avenue, which several recent studies have begun exploring. For instance, OT has been incorporated into neural architecture search (NAS) pipelines [Yang et al., 2023, Nguyen et al., 2020, Kandasamy et al., 2018], as well as into knowledge distillation techniques for training shallower student networks [Lohit and Jones, 2020, Chen et al., 2020].

We join in this line of work, deploying OT to develop a DNN depth reduction strategy. However, conversely, to these approaches, our strategy does not involve the training of more than one network but rather operates intra-model. OT tools are used in our case to render the distributional changes inside the same model allowing us to strategically and efficiently quantify and control its learning redundancy. Overall, our contributions can be summarized as follows:

- We propose a novel OT-based and block collapse inductive regularization (Sec. 3), seamlessly integrated into the main training pipeline of neural networks. Our approach consists of augmenting the conventional loss function for a standard classification task, given a dataset, with blockwise OT discrepancy measure, specifically the Max-Sliced Wasserstein distance, between the input and output features’ probability distributions of the blocks forming the network (Sec. 3.2.3).
- We motivate our strategy (Sec. 3.2.1 and Sec. 3.2.2), showing how it allows, post-training, for the complete removal of several blocks from the architecture at once.
- Our proposed regularization strategy shows its effectiveness in reducing the depth of overparametrized DNNs with marginal performance loss with respect to competing state-of-the-art techniques (Sec. 4.2).

2 Related Works

Neural Network Depth Reduction. Several approaches have been designed to strategically prune layers from the neural networks and reduce their depth. Yang et al. [2024] observed a high degree of similarity between consecutive layers in transformer-based models and proposed a layer-pruning strategy that leverages the augmentation of a layer’s parameters with the cumulative differences between the considered layer and a set of subsequent layers. Gromov et al. [2024] also highlight the high redundancy level, especially for deeper layers, and therefore proceed to consecutively prune layers starting from the penultimate, followed by a fine-tuning step to recover the performance. Other activation-based structured pruning approaches invoke strategies of ranking and layer importance estimation, such as feature representation assessment [Chen and Zhao, 2019] or layer entropy evaluation [Liao et al., 2023, 2024, Quéту et al., 2024], aiming to identify and remove the least important layers, with subsequent performance recovery through transfer learning. A major difference with our work is that these approaches proceed upon the identification of suitable removable layers and operating their collapse in such a way that the performance of the model is tolerably affected. Hence, our strategy improves over them as it induces the collapse during the training, of a stack of layers at once. Also, these approaches either involve a prior fixing of the number of layers to be pruned or rely on ranking criteria, which is not the case in our approach, as the training procedure naturally leads to the identification of the least important blocks in the architecture, which will be suitable for removal.

Layer folding is yet another strategy, introduced in Dror et al. [2021], entailing a training scheme that forces certain activations to remain either linear or non-linear, facilitating the merging of corresponding adjacent layers. While promising, this technique requires additional training to learn the linearization parameter.

Knowledge distillation presents another line of work, involving training a smaller, shallower network (the student) from a deeper network (the teacher) [Hinton et al., 2015]. Certain approaches even incorporate an OT regularized loss into the training of the student network [Lohit and Jones, 2020, Chen et al., 2020] to achieve a better quantification of the distance between the student and the teacher.

Neural architecture search (NAS) techniques seek to reduce network depth by identifying the optimal architecture for a given task. Methods like OT-based NAS [Nguyen et al., 2020] leverage OT to characterize the distance between neural network architectures, often relying on a graph-theoretic formalism. OT’s ability to capture distance and discern differences in features among structured objects makes it promising for NAS.

However, overall, existing knowledge distillation and NAS approaches typically involve training multiple separate neural networks, a limitation addressed in our work, which allows for depth reduction of the considered neural network and, subsequently of its training.

Distribution discrepancy metrics. The problem of characterizing distribution discrepancy has been a long-standing challenge in machine learning and statistics. Various metrics have been employed to tackle diverse deep-learning tasks. For instance, Kullback-Leibler (KL) divergence has been widely used in generative modeling tasks, albeit it solely captures pointwise differences between probability distributions and is intrinsically limited when the probabilities exhibit disjoint support. Furthermore, KL divergence fails to encapsulate the geometric structure of the distributions. To address these limitations, alternative discrepancy measures have been developed to better capture the geometry of probability distributions. The minimum mean discrepancy (MMD) and central moment discrepancy (CMD) [Zellinger et al., 2017, Kalischek et al., 2021] for example, both moment-matching strategies, have been introduced to facilitate distribution matching, although they might suffer from some practical drawbacks, such as the vanishing gradient problem at extreme points of the feature space.

Another prominent metric in this category is the Wasserstein distance, which is an OT distance that quantifies the minimal transformation between two distributions of points based on a specified transportation cost [Peyré and Cuturi, 2018]. Owing to its ability to mitigate vanishing gradients, the Wasserstein distance has been successfully applied in various domains, including generative modeling for training GANs and autoencoders [Rabin and Peyré, 2011, Frogner et al., 2015], as well as domain adaptation [Lee et al., 2019] and style transfer [Heitz et al., 2021], where quantifying distribution distances is essential. However, Wasserstein distance-based GANs often suffer from the "curse of dimensionality," leading to instability and complexity issues. To alleviate this problem, sliced versions of the 2-Wasserstein distance have been proposed as a remedy. These methods entail estimating distances of 1-D distributions only, thereby circumventing the aforementioned limitations [Wu et al., 2019, Kolouri et al., 2019, Nguyen and Ho, 2022, Tanguy et al., 2023]. In Vayer and Gribonval [2021], it has been shown that controlling the Wasserstein distance yields control over MMD under mild constraints. Thus in our work, we leverage the optimal transport paradigm, particularly sliced Wasserstein distances, to account for distributional discrepancies.

Relation to other Wasserstein-regularized training frameworks. In Karkar et al. [2020], a Wasserstein regularization of the loss is investigated and its generalization-enhancing impact is highlighted. In Karkar et al. [2023] a similar scheme is used to achieve greedy module-wise training. This regularization method penalizes the kinetic energy of the modules, encouraging them to maintain the geometry of the problem and prevent overfitting, preserving crucial information for later stages.

Besides, Joo et al. [2020] propose a projected error function regularization of the loss, derived as an upper bound on the sliced Wasserstein distance. Their goal is to regularize activations in the Wasserstein probability distributions' space during the training by pushing their distribution to be close to the standard normal distribution, serving as a replacement for the conventional use of batch normalization layers. Overall, our method builds upon a similar concept by employing a sliced variant of the Wasserstein distance as a regularizer during training, but the distance is computed between blocks in the same network and we rather use it to selectively prune blocks from the neural network architecture and reduce its depth in the post-training phase, ultimately yielding a more efficient and streamlined model.

3 Method

In this section, we begin by offering a concise but useful overview of optimal transport theory (Sec. 3.1) and defining the adopted learning framework (Sec. 3.2). Next, we detail our method for reducing neural network depth using optimal transport (Sec. 3.2.1): we introduce a regularization strategy based on the Max-Sliced Wasserstein distance to minimize the distance between intermediate feature distributions in the neural network. Fig. 1 provides a general overview of our method. We also present some insights into this strategy and how it allows for the removal of intermediate layers in the network after training, with in principle minimal performance degradation (Sec. 3.2.2).

3.1 Background on Optimal Transport

In this subsection, we present a succinct overview of OT and the Wasserstein distance for discrete distributions [Peyré and Cuturi, 2018].

Given two metric spaces \mathcal{X} and \mathcal{Y} and a cost function c defined over $\mathcal{X} \times \mathcal{Y}$, the goal of the OT problem is to determine the most efficient manner to transport mass from one distribution, defined over \mathcal{X} to another supported over \mathcal{Y} , where the transportation cost is dictated by the chosen function c .

For $\mathcal{X} = \mathcal{Y} = \mathbb{R}^d$, we consider two discrete probability measures and we recall the **Monge Formulation of the OT problem**:

$$OT(\mu, \nu, c) = \min_T \sum_i c[\mathbf{x}_i, T(\mathbf{x}_i)], \quad (1)$$

where μ and ν defined as

$$\mu = \sum_{i=1}^N \alpha_i \delta_{\mathbf{x}_i}, \quad \nu = \sum_{i=1}^M \beta_i \delta_{\mathbf{y}_i}, \quad (2)$$

where δ_x refers to the Dirac (unit mass) distribution at point \mathbf{x} . The weights α and β reside in the probability simplex $\{a \in \mathbb{R} \mid \sum a_i = 1\}$, and T is defined as $T : \{\mathbf{x}_1, \dots, \mathbf{x}_N\} \rightarrow \{\mathbf{y}_1, \dots, \mathbf{y}_M\}$ and verifying

$$\beta_j = \sum_{i:T(\mathbf{x}_i)=\mathbf{y}_j} \alpha_i, \quad \forall j \in \llbracket M \rrbracket, \quad (3)$$

or more compactly $T_{\#}\mu = \nu$.

In the following, we will consider only the case of uniform weights and the same support size, taking $M = N$ and $\alpha_i = \beta_j = \frac{1}{N}$. We also take as the cost function $c(\mathbf{x}, \mathbf{y}) = \|\mathbf{x} - \mathbf{y}\|_p^p$ for $\mathbf{x} \in \mathcal{X}$, $\mathbf{y} \in \mathcal{Y}$, $p \in \mathbb{R}_{>0}$. In this case, OT establishes a measure of distance between the probability distributions. Such a distance, known as the **p-Wasserstein distance**, is in general defined as $\mathcal{W}_p = OT(\mu, \nu, c)^{\frac{1}{p}}$. When we have the dimension of the ground space being $d = 1$, the Wasserstein distance takes on a closed form, given by

$$\mathcal{W}_p = \left(\frac{1}{N} \sum_{i=1}^N |\mathbf{x}_i - \mathbf{y}_i|^p \right)^{\frac{1}{p}}, \quad (4)$$

where we assume $x_1 < \dots < x_N$ and $y_1 < \dots < y_N$ such that $\mathbf{x}_i \mapsto \mathbf{y}_i, \forall i$.

Given the closed-form expression in one dimension, sliced variants of the Wasserstein distance have been introduced. These variants transform sample assignment and distance calculation by sorting the one-dimensional projection of the samples. This process yields a sufficient approximation of the high-dimensional Wasserstein distance, which is immune to the curse of dimensionality [Si et al., 2020]. Specifically, our focus lies on the **p-Max-Sliced Wasserstein distance**, introduced in Deshpande et al. [2019], and defined as follows:

$$\text{Max-SWD}_p(\mu, \nu) = \max_{\theta \in \mathcal{U}(\mathbb{S}^{d-1})} \mathcal{W}_p(\theta_{\#}\mu, \theta_{\#}\nu), \quad (5)$$

where $\theta_{\#}$ stands for the pushforwards of the projection $X : \mathbb{R}^d \mapsto \langle \theta, X \rangle$, $\langle \cdot, \cdot \rangle$ for the dot product operator and $\mathcal{U}(\mathbb{S}^{d-1})$ for the uniform distribution on the unit hyper-sphere of dimension $d - 1$.

Essentially, the Max-Sliced Wasserstein distance represents a version of the sliced Wasserstein distance where we select the optimal direction to project the probability measures, i.e. the direction along which the projected distance is maximized, also possessing valid metric properties [Nadjahi et al., 2020, 2021] [Bonneel et al., 2015]. In our work, we will consider the Max-Sliced Wasserstein distance, for its previously discussed convenience, specifically computed for $p = 2$, to quantify the distance between intermediate probability distributions between blocks inside a neural network model, as it will be presented in the next section.

3.2 Learning Framework

In this subsection, we introduce our learning framework. Let us define $\mathcal{T} = T_K \circ \dots \circ T_1$ as the DNN we wish to train on the dataset \mathcal{D} , where each T_k is an elementary module (which can be defined as single or multiple layers). Given a loss function \mathcal{L} we aim at minimizing, the objective entails minimizing the problem

$$(\mathcal{T}, F) \in \arg \min_{\mathcal{T}, F} \sum_{i=1}^{|\mathcal{D}|} \mathcal{L}[(F \circ \mathcal{T})(\mathbf{x}_{1,i}), y_i], \quad (6)$$

where F is a classifier layer, $\mathbf{x}_{1,i}$ is the i -th input sample for the DNN, and y_i is the associated ground-truth label and $|\mathcal{D}|$ indicates the number of samples in the dataset.

For each module T_k we consider the *input probability distribution* to be $\mu_k := \frac{1}{|\mathcal{D}|} \delta_{\mathbf{y}_{k-1, \mathcal{D}}} = \frac{1}{|\mathcal{D}|} \delta_{\mathbf{x}_{k, \mathcal{D}}} = \sum_{i=1}^{|\mathcal{D}|} \delta_{\mathbf{x}_{k,i}}$ (being the output of the preceding module T_{k-1}), and similarly the *output probability distribution* $\nu_k := \delta_{\mathbf{y}_{k, \mathcal{D}}} = \sum_{i=1}^{|\mathcal{D}|} \delta_{\mathbf{y}_{k,i}}$

According to our notation, $\nu_k \equiv \mu_{k+1}$, given that $\mathbf{y}_{k,i} = \mathbf{x}_{k+1,i} \forall i, k$. Furthermore, we assume that $\mathbf{x}_{k,i}$ and $\mathbf{y}_{k,i}$ possess identical dimensions, and consequently μ_k and ν_k to live in the same dimensional space, allowing for the computation of the distance between them. In the following, our goal would in fact be to control these distances during training so as to allow for the isolation and removal of certain blocks post-training, with almost no loss of performance.

3.2.1 Proposed Regularization

Our objective is to reduce the depth of the neural network. To achieve such a goal, we will incorporate a penalization of the distance between two consecutive blocks during training. This is to assist the DNN in learning a target input-output function \mathcal{T} while following the shortest path. This yields, after training, to identify blocks that can be removed from the architecture without impacting the performance. Specifically, these blocks introduce marginal statistical modification on their corresponding input features. Including this constraint to the learning translates into minimizing, besides the loss \mathcal{L} , a regularizer

$$\mathcal{R} = \frac{1}{K} \sum_{k=1}^K \text{Max} - \text{SWD}_2(\hat{\mu}_k, \hat{\nu}_k), \quad (7)$$

where the probability distributions $\hat{\mu}_k$ and $\hat{\nu}_k$ are the empirical counterparts of the previously defined distributions μ_k and ν_k . They are constructed over uniformly-weighted samples of a N -sized minibatch, and so defined by $\hat{\mu}_k = \frac{1}{N} \sum_{i=1}^N \delta_{\mathbf{x}_{k,i}}$, where $\mathbf{x}_{k,i}$ is taken as the flattened input vector of the block corresponding to the i -th element of the minibatch.

Post-training, if the distance $\widehat{\mathcal{R}}_k := \text{Max} - \text{SWD}_2(\hat{\mu}_k, \hat{\nu}_k)$ falls below a fixed threshold ε , the corresponding block T_k can be pruned from the architecture. Namely, this threshold is related to a tolerated performance drop budget δ fixed a priori.

Motivation. We build upon the demonstration of Karkar et al. [2020, 2023] and Gai and Zhang [2021]: training a neural network can be formulated as an optimization problem in the Wasserstein space, where deep neural networks tend to approximate geodesic curves.

The regularization in (7) aims to minimize the distances between the input and output distributions of the blocks forming the architecture during training. The DNN learns while adhering to a least action principle [Karkar et al., 2020], incentivized to avoid unnecessary distributional changes throughout the learning process. By favoring solutions aligned with this principle, efficiency in training is promoted in the sense that the data is transported in a way that preserves and simplifies the patterns in the input distribution. We encourage this behavior to enable the removal of certain blocks of the architecture after training is concluded, thus reducing its depth and alleviating the computational burden during inference.

Let us assume, for some k , to have nullified the regularization term: we have

$$\text{Max} - \text{SWD}_2(\mu_k, \nu_k) = \text{Max} - \text{SWD}_2(\mu_k, T_{k\#}\mu_k) = 0 \Rightarrow \mu_k = T_{k\#}\mu_k = \nu_k, \quad (8)$$

and since in our setup $T_k = (\text{Id} + f_k)$, this results in having $f_{k\#}\mu_k = 0$ and $T_{k\#} = \text{Id}$.

3.2.2 Properties of the proposed regularization

The regularization acts similarly to a soft 1-Lipschitz constraint. By looking closer into μ_k and ν_k (the input and output distributions of the k -th block), the central limit theorem suggests that μ_k can be regarded asymptotically as a Gaussian distribution with mean \mathbf{m}_k and covariance Σ_k . Then, by employing the delta method, ν_k can be approximated asymptotically as a Gaussian distribution with mean $T_k(\mathbf{m}_k)$ and covariance $J_k^T \Sigma_k J_k$, where J_k represents the Jacobian matrix of the block transformation T_k .

The constraint $\mu_k = \nu_k$ can then be interpreted as an orthogonality constraint on the Jacobian of the block transformation, indicating that our regularization imposes a similar effect as enforcing orthogonality on the Jacobian. This implies a block-wise soft Lipschitz constraint on the neural network by preserving gradient norms that drive the network to be 1-Lipschitz. This type of constraint was thoroughly investigated in the literature [Li et al., 2019, Anil et al., 2018, Béthune et al., 2022] and it has been particularly shown in Béthune et al. [2022] that a 1-Lipschitz constraint does not limit the expressiveness, i.e the capacity and learning flexibility of a neural network, for classification tasks. Instead, this regularization should offer a different stance on the tradeoff between generalization and accuracy. This also coincides with the results in Karkar et al. [2020] that highlight the generalization-enhancing effect of such a regularization. During training, provided that a proper weight on the regularization (through some hyperparameter λ) is tuned, the neural network’s expressive power should in principle remain intact, while adhering to the least action principle, thereby preventing arbitrary amplification of small differences and big distributional changes.

Stationary point analysis. The whole optimization problem can be expressed as:

$$\mathcal{J} = \mathcal{L} + \lambda \mathcal{R} \Rightarrow \frac{\partial \mathcal{J}}{\partial w_{k_0}} = \frac{\partial \mathcal{L}}{\partial w_{k_0}} + \lambda \frac{\partial \mathcal{R}}{\partial w_{k_0}}, \quad k_0 \in \llbracket K \rrbracket \quad (9)$$

Algorithm 1 Our proposed method LaCoOT.

```

1: function LACOOT( $\mathbf{w}^{\text{INIT}}, \mathcal{D}, \lambda, \delta$ )
2:    $\mathbf{w} \leftarrow \text{Train}(\mathbf{w}^{\text{init}}, \mathcal{D}_{\text{train}}, \lambda)$ 
3:    $\text{dense\_acc} \leftarrow \text{Evaluate}(\mathbf{w}, \mathcal{D}_{\text{val}})$ 
4:    $\text{current\_acc} \leftarrow \text{dense\_acc}$ 
5:   while ( $\text{dense\_acc} - \text{current\_acc}$ ) >  $\delta$  do
6:      $\widehat{\mathcal{R}} = [\widehat{\mathcal{R}}_1, \widehat{\mathcal{R}}_2, \dots, \widehat{\mathcal{R}}_K]$  ▷ Max-Sliced Wasserstein Distance calculation on  $\mathcal{D}_{\text{val}}$ 
7:      $l \leftarrow \text{argmin}(\widehat{\mathcal{R}})$  ▷ Finding the lowest Wasserstein Distance
8:      $T_l = \text{Identity}()$  ▷ Replacement of the layer with an Identity
9:      $\text{current\_acc} \leftarrow \text{Evaluate}(\mathbf{w}, \mathcal{D}_{\text{val}})$  ▷ Re-evaluation on  $\mathcal{D}_{\text{val}}$ 
10:  end while
11:  return  $\mathbf{w}$ 
12: end function

```

where λ is a positive hyper-parameter. We then characterize the stationary point as:

$$\frac{\partial \mathcal{L}}{\partial w_{k_0}} + \lambda \frac{\partial \mathcal{R}}{\partial w_{k_0}} = 0 \Rightarrow \lambda = -\frac{\partial \mathcal{L}}{\partial w_{k_0}} \cdot \frac{1}{\frac{\partial \mathcal{R}}{\partial w_{k_0}}}. \quad (10)$$

From this equation, since $\lambda \geq 0$, we clearly observe that the loss and the regularizer are antagonists. Hence, while browsing the parameter space to minimize the loss, unrestricted DNNs are rather biased towards increasing intermediate distributional changes in the path they take. These changes, which can namely be evaluated when taking the inter-block distances in the vanilla setting, might be irrelevant: the DNN can converge to another local minimum in the loss landscape, with similar performance but without undergoing too many distributional changes.

In the learning process, we recall though that the primary objective is to traverse the gap between the input distribution and the target output distribution. A crucial threshold is thus reached when the network’s output converges to the ground truth. Namely, this inherent distance between the input and ground truth distribution defines a tight lower bound for the regularization value, corresponding to the minimal distributional changing capacity that still has to be maintained in the network to have a good performance and not to underfit. This is guaranteed by applying the Triangle inequality:

$$\text{Max} - \text{SWD}_2(\mu_1, \nu_{GT}) \leq \sum_{k=1}^K \text{Max} - \text{SWD}_2(\mu_k, \nu_k) + \text{Max} - \text{SWD}_2(\nu_K, \nu_{GT}), \quad (11)$$

where ν_{GT} denotes the ground truth distribution of the labels.

3.2.3 Overview on the Procedure

Depicted in Alg. 1 in the Appendix, we present here LaCoOT to remove the layers having the lowest Max-Sliced Wasserstein distances. Indeed, the layer having the lowest Max-Sliced Wasserstein distance is likely to have a function close to the identity function. Therefore, this layer can be linearized, as keeping it is unnecessary. Aiming at this, we first train the neural network, represented by its weights at initialization \mathbf{w}^{init} , on the training set $\mathcal{D}_{\text{train}}$ with our regularization set by λ (line 2) and evaluate it on the validation set \mathcal{D}_{val} (line 3). We then calculate the Max-Sliced Wasserstein distance $\widehat{\mathcal{R}}_k$ for each considered layer k for all the K considered layers (line 6). We then find the layer having the lowest Max-Sliced Wasserstein distance (line 7) and replace it with the Identity (line 8). In the following steps, this layer is, obviously, no longer taken into consideration. The performance of the model is re-evaluated on the validation set \mathcal{D}_{val} (line 9). Once the performance on the validation set drops below the threshold δ , the final model is obtained.

4 Experiments

In this section, we empirically evaluate the effectiveness of our proposed approach, across multiple architectures and datasets for traditional image classification setups.

4.1 Experimental setup

We assess our approach LaCoOT on three widely used models, ResNet-18, MobileNet-V2, and Swin-T trained on seven different datasets: CIFAR-10 Krizhevsky et al. [2009], Tiny-ImageNet Le and Yang [2015], PACS and VLCS from

Dataset	Approach	ResNet-18		Swin-T		MobileNetv2	
		top-1[%]	MACs(↓)	top-1[%]	MACs(↓)	top-1[%]	MACs(↓)
CIFAR-10	Original	91,77	140,19 M	91,67	518,94 M	93,50	87,98 M
	LaCoOT ($\lambda = 0$)	64,46	64,69 M	79,15	492,17 M	81,41	87,51 M
	LaCoOT (λ_{LOW})	89,01	64,69 M	83,24	492,17 M	84,64	87,29 M
	LaCoOT (λ_{HIGH})	90,99	64,69 M	81,48	492,17 M	84,87	86,98 M
Tiny ImageNet 200	Original	41,48	148,15 M	75,48	772,45 M	45,92	24,7 M
	LaCoOT ($\lambda = 0$)	31,56	91,53 M	72,74	720,83 M	32,72	24,59 M
	LaCoOT (λ_{LOW})	40,18	91,53 M	72,76	720,83 M	37,78	24,51 M
	LaCoOT (λ_{HIGH})	39,30	91,53 M	72,92	720,83 M	40,68	24,37 M
PACS	Original	79,10	6,87 G	97,00	4,5 G	95,40	299,51 M
	LaCoOT ($\lambda = 0$)	52,00	5,94 G	91,70	3,76 G	50,70	297,81 M
	LaCoOT (λ_{LOW})	57,30	5,94 G	93,20	3,76 G	61,70	298,15 M
	LaCoOT (λ_{HIGH})	63,80	5,02 G	93,70	3,76 G	84,90	297,47 M
VLCS	Original	69,06	6,87 G	83,04	4,5 G	80,90	299,51 M
	LaCoOT ($\lambda = 0$)	55,55	5,94 G	81,08	3,76 G	57,04	298,82 M
	LaCoOT (λ_{LOW})	56,38	5,94 G	80,80	3,76 G	66,45	298,82 M
	LaCoOT (λ_{HIGH})	60,58	5,02 G	81,64	3,76 G	79,22	298,82 M
Flowers 102	Original	89,31	1,81 G	92,19	4,5 G	91,10	299,51 M
	LaCoOT ($\lambda = 0$)	51,08	1,35 G	90,89	4,13 G	51,46	298,95 M
	LaCoOT (λ_{LOW})	52,89	1,35 G	91,12	4,13 G	81,17	298,95 M
	LaCoOT (λ_{HIGH})	62,14	1,35 G	91,07	4,13 G	84,32	298,95 M
DTD	Original	61,38	1,81 G	68,51	4,5 G	63,94	299,51 M
	LaCoOT ($\lambda = 0$)	55,43	1,58 G	65,37	4,12 G	53,24	298,88 M
	LaCoOT (λ_{LOW})	54,31	1,58 G	66,97	4,13 G	52,77	298,88 M
	LaCoOT (λ_{HIGH})	57,18	1,58 G	65,00	4,12 G	56,33	298,88 M
Aircraft	Original	74,32	1,81 G	78,16	4,5 G	74,38	299,51 M
	LaCoOT ($\lambda = 0$)	61,33	1,58 G	74,35	4,12 G	46,44	298,94 M
	LaCoOT (λ_{LOW})	59,83	1,58 G	73,00	4,12 G	51,25	298,94 M
	LaCoOT (λ_{HIGH})	62,98	1,58 G	74,17	4,12 G	64,00	298,94 M

Table 1: Test performance (top-1) and MACs for all the considered setups. Original refers to the trained model without layer deletion. To highlight the effectiveness of our method concerning the performance/compressibility tradeoff, results for LaCoOT are reported with two different λ . The best results between LaCoOT ($\lambda = 0$), LaCoOT (λ_{LOW}), and LaCoOT (λ_{HIGH}) are in **bold**.

DomainBed Gulrajani and Lopez-Paz [2020], as well as Flowers-102 Nilsback and Zisserman [2008], DTD Cimpoi et al. [2014], and Aircraft Maji et al. [2013]. All the hyperparameters, augmentation techniques, and learning policies are presented in Appendix, mostly following Quéto and Tartaglione [2024] and Quéto et al. [2024]. We also use the implementation of the Max Sliced Wasserstein distance available in the POT toolbox [Flamary et al., 2021]. To calculate the Max-Sliced Wasserstein distance, the two distributions must have the same dimensions. Hence, not all the layers can be considered removable with our method. For ResNet-18, we consider four removable blocks, each of them corresponding to the second Basic Block.¹ For Swin-T, the twelve Swin Transformer blocks are taken into account. Finally, the twelve blocks composed of convolutional, batchnorm, and ReLU layers are considered removable for MobileNetv2.

4.2 Results

Table 1 shows the test performance (top-1) associated with the required Multiply-Accumulate operations (MACs) for inference on one image for all the considered setups. For each combination of dataset and architecture, more results are shown in the tables in the Appendix.

In most of the setups, we can observe the effectiveness of our method. First, blindly applying our method to a model trained without training the model with our proposed regularization (LaCoOT ($\lambda = 0$)) consistently leads to worse

¹We recall that ResNet-18 is composed of a sequence of 8 Basic Blocks in pairs. Each Basic Block is composed of a sequence of convolutional, batchnorm, and ReLU layers repeated twice.

results compared to cases where our regularization is applied. Moreover, in general, applying LaCoOT with a high regularization (λ_{HIGH}) results in models with fewer multiply-accumulate operations and better performance. For example, this is the case for ResNet-18 on VLCS, where 15% fewer operations compared to LaCoOT (λ_{LOW}) are needed for more than 4% improvement in accuracy.

The Swin-T case. Interestingly, Swin-T naturally possesses blocks that can be removed with almost no performance loss. This behavior can be linked to recent works such as Gromov et al. [2024], Yang et al. [2024], Men et al. [2024] observed in large language models, where naturally the last layers are not needed in the model, and removing them does not impact the performance. This natural behavior may be at the root of the difficulty in regularizing Swin-T properly with our LaCoOT method.

Comparison with the original model. Although in certain setups, such as ResNet-18 on CIFAR-10, LaCoOT effectively reduces model size while maintaining the original model’s performance, it often results in some performance degradation compared to the original model. This is likely because the model is not re-trained after layer removal. In contrast, traditional compression schemes typically involve re-training the model after dropping some parameters to recover performance.

4.3 Ablation Study

In this subsection, we compare LaCoOT with two baseline methods². The first method, which we call "BI", evaluates the impact of the deletion of a layer on performance. Indeed, layers are removed in ascending order of their impact on performance, with those that do not affect performance being removed first, and those that do affect performance the most being removed last. Thus, this method achieves the theoretical best model. The second method, which we refer to as "Random", iteratively removes layers in random order. Based on randomness, error bars have been calculated on 10 seeds. Fig. 2 shows this comparison on a ResNet-18 on CIFAR-10.

First, in the absence of regularization during training (i.e., with $\lambda = 0$), we can observe that the Max-Sliced Wasserstein distance as such, is not a faithful indicator of block importance, since it can be surpassed by random block removal. Considering our previous theoretical analysis, this observation is largely expected. Indeed, unrestricted DNN blocks tend to operate significant, yet irrelevant changes in their intermediate probability distributions of the features, during training as explained in 3.2.2. Formally, the Wasserstein metric quantifies the difference between the input and output distributions of the block rather than providing an intrinsic importance measure. However, when the metric is incorporated into the training process, it gains a meaningful interpretation. By encouraging the DNN to learn while minimizing distributional changes during training, the distance can be seen afterward as a measure of the minimal necessary distributional modifications operated by the block to minimize the loss function for the specific task, thereby providing a more reliable basis for importance ranking of the model blocks. Indeed, we can observe that LaCoOT ($\lambda = 5$) halves the number of MACs with almost no performance drop with respect to the dense model. Moreover, LaCoOT achieves a better performance/compression trade-off compared to the two baseline methods Block Influence and Random.

4.4 Limitations and Future Work

While effective in alleviating the computational burden of DNNs, LaCoOT also possesses some limitations, as discussed below.

Performance degradation. Compressing existing parameter-efficient architectures is particularly challenging, and LaCoOT cannot reduce the depth of an already underfitted architecture without compromising performance, as seen with MobileNetv2 on Tiny-ImageNet-200. However, it achieves effective reduction of the depth of overfitted DNNs,

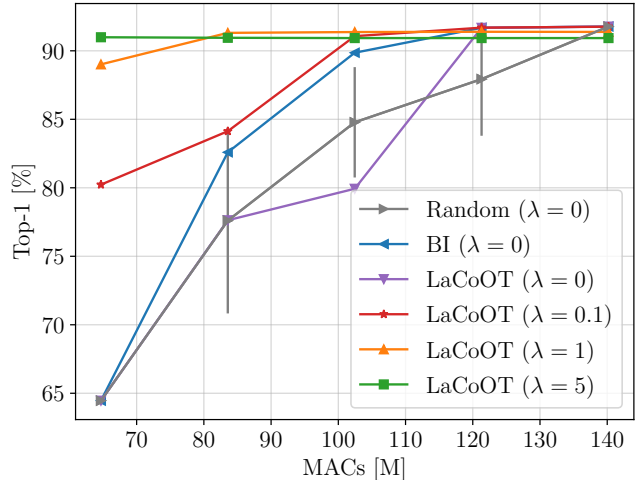


Figure 2: Comparison of LaCoOT, BI (theoretical best), and Random for ResNet-18 on CIFAR-10. LaCoOT ($\lambda = 5$) halves the MACs with minimal performance loss. Higher λ values further reduce MACs while maintaining performance.

²We also compare LaCoOT with existing approaches in Sec. D in Appendix.

especially given that only one training session is required to achieve compression.

Layers targeted by LaCoOT. Not all layers can be targeted and removed by LaCoOT. To calculate the Max-Sliced Wasserstein distance between two distributions, they must be of the same size. This means that certain layers, such as convolutional layers that increase the number of filters or reduce the size of features, cannot be targeted by LaCoOT. A potential solution to explore would be to perform zero padding on the distribution that has the smallest dimension, in order to match the dimension of the second distribution. Although it seems simple, this case is not trivial, as the properties of the Wasserstein metric can be lost by applying zero padding [Cai and Lim, 2020]. This exploration is therefore left to future work.

5 Conclusion

In this work, we have proposed LaCoOT, a new optimal transport based regularization strategy, specifically using the Max-Sliced Wasserstein metric to minimize the distances between the intermediate feature distributions in the neural network. This regularization enables, post-training, the complete removal of layers from the architecture with a minor impact on performance. Experiments conducted on three widely used architectures across seven image classification datasets have demonstrated LaCoOT’s capability and effectiveness in reducing the number of layers in the neural network. Concerned about the increasing environmental impact of AI, we hope this work will inspire future optimization techniques and new approaches for network compression.

References

- C. H. Ali Mehmeti-Göpel and J. Disselhoff. Nonlinear advantage: trained networks might not be as complex as you think. In *Proceedings of the 40th International Conference on Machine Learning (ICML)*, 2023.
- C. Anil, J. Lucas, and R. B. Grosse. Sorting out lipschitz function approximation. In *International Conference on Machine Learning (ICML)*, 2018.
- D. Baymurzina, E. Golikov, and M. Burtsev. A review of neural architecture search. *Neurocomputing*, 2022.
- L. Béthune, T. Boissin, M. Serrurier, F. Mamalet, C. Friedrich, and A. G. Sanz. Pay attention to your loss : understanding misconceptions about lipschitz neural networks. In *Advances in Neural Information Processing Systems (NeurIPS)*, 2022.
- N. Bonneel, J. Rabin, G. Peyré, and H. Pfister. Sliced and Radon Wasserstein Barycenters of Measures. *Journal of Mathematical Imaging and Vision*, 2015.
- Y. Cai and L.-H. Lim. Distances between probability distributions of different dimensions. *IEEE Transactions on Information Theory*, 2020.
- L. Chen, Z. Gan, D. Wang, J. Liu, R. Henao, and L. Carin. Wasserstein contrastive representation distillation. *2021 IEEE/CVF Conference on Computer Vision and Pattern Recognition (CVPR)*, 2020.
- S. Chen and Q. Zhao. Shallowing deep networks: Layer-wise pruning based on feature representations. *IEEE Transactions on Pattern Analysis and Machine Intelligence*, 2019.
- M. Cimpoi, S. Maji, I. Kokkinos, S. Mohamed, , and A. Vedaldi. Describing textures in the wild. In *CVPR*, 2014.
- I. Deshpande, Y.-T. Hu, R. Sun, A. Pyrros, N. Siddiqui, O. Koyejo, Z. Zhao, D. A. Forsyth, and A. G. Schwing. Max-sliced wasserstein distance and its use for gans. *2019 IEEE/CVF Conference on Computer Vision and Pattern Recognition (CVPR)*, 2019.
- A. B. Dror, N. Zehngut, A. Raviv, E. Artyomov, R. Vitek, and R. J. Jevnisek. Layer folding: Neural network depth reduction using activation linearization. In *British Machine Vision Conference (BMVC)*, 2021.
- R. Flamary, N. Courty, A. Gramfort, M. Z. Alaya, A. Boisbunon, S. Chambon, L. Chapel, A. Corenflos, K. Fatras, N. Fournier, L. Gautheron, N. T. Gayraud, H. Janati, A. Rakotomamonjy, I. Redko, A. Rolet, A. Schutz, V. Seguy, D. J. Sutherland, R. Tavenard, A. Tong, and T. Vayer. Pot: Python optimal transport. *Journal of Machine Learning Research (JMLR)*, 2021.
- C. Frogner, C. Zhang, H. Mobahi, M. Araya, and T. A. Poggio. Learning with a wasserstein loss. In *Advances in Neural Information Processing Systems (NeurIPS)*, 2015.
- K. Gai and S. Zhang. A mathematical principle of deep learning: Learn the geodesic curve in the wasserstein space. *ArXiv*, 2021.
- A. Gromov, K. Tirumala, H. Shapourian, P. Glorioso, and D. A. Roberts. The unreasonable ineffectiveness of the deeper layers. *ArXiv*, 2024.

- I. Gulrajani and D. Lopez-Paz. In search of lost domain generalization. In *ICLR*, 2020.
- S. Han, J. Pool, J. Tran, and W. Dally. Learning both weights and connections for efficient neural network. In *Advances in Neural Information Processing Systems (NeurIPS)*, 2015a.
- S. Han, J. Pool, J. Tran, and W. Dally, 2015b.
- K. He, X. Zhang, S. Ren, and J. Sun. Delving deep into rectifiers: Surpassing human-level performance on imagenet classification. In *2015 IEEE International Conference on Computer Vision (ICCV)*, 2015.
- Y. He and L. Xiao. Structured pruning for deep convolutional neural networks: A survey. *IEEE transactions on pattern analysis and machine intelligence*, 2023.
- E. Heitz, K. Vanhoey, T. Chambon, and L. Belcour. A sliced wasserstein loss for neural texture synthesis. In *IEEE/CVF Conference on Computer Vision and Pattern Recognition (CVPR)*, 2021.
- K. Hermann, H. Mobahi, T. FEL, and M. C. Mozer. On the foundations of shortcut learning. In *The Twelfth International Conference on Learning Representations (ICLR)*, 2024.
- G. E. Hinton, O. Vinyals, and J. Dean. Distilling the knowledge in a neural network. *ArXiv*, 2015.
- S. Ioffe and C. Szegedy. Batch normalization: Accelerating deep network training by reducing internal covariate shift. In *Proceedings of the 32nd International Conference on Machine Learning (ICML)*, 2015.
- T. Joo, D. Kang, and B. Kim. Regularizing activations in neural networks via distribution matching with the wasserstein metric. In *International Conference on Learning Representations (ICLR)*, 2020.
- N. Kalischek, J. Wegner, and K. Schindler. In the light of feature distributions: moment matching for neural style transfer. In *2021 IEEE/CVF Conference on Computer Vision and Pattern Recognition (CVPR)*, 2021.
- K. Kandasamy, W. Neiswanger, J. Schneider, B. Poczos, and E. P. Xing. Neural architecture search with bayesian optimisation and optimal transport. In *Advances in Neural Information Processing Systems (NeurIPS)*, 2018.
- S. Karkar, I. Ayed, E. de Bezenac, and P. Gallinari. A Principle of Least Action for the Training of Neural Networks. In *European Conference on Machine Learning and Principles and Practice of Knowledge Discovery in Databases (ECML PKDD)*, 2020.
- S. Karkar, I. Ayed, E. de Bézenac, and P. Gallinari. Module-wise training of neural networks via the minimizing movement scheme. In *Advances in Neural Information Processing Systems (NeurIPS)*, 2023.
- S. Kolouri, P. E. Pope, C. E. Martin, and G. K. Rohde. Sliced wasserstein auto-encoders. In *International Conference on Learning Representations (ICLR)*, 2019.
- A. Krizhevsky, G. Hinton, et al. Learning multiple layers of features from tiny images, 2009.
- Y. Le and X. Yang. Tiny imagenet visual recognition challenge. *CS 231N*, 7(7):3, 2015.
- C.-Y. Lee, T. Batra, M. H. Baig, and D. Ulbricht. Sliced wasserstein discrepancy for unsupervised domain adaptation. *2019 IEEE/CVF Conference on Computer Vision and Pattern Recognition (CVPR)*, 2019.
- Q. Li, S. Haque, C. Anil, J. Lucas, R. B. Grosse, and J.-H. Jacobsen. Preventing gradient attenuation in lipschitz constrained convolutional networks. *Advances in Neural Information Processing Systems (NeurIPS)*, 2019.
- S. Liang and R. Srikant. Why deep neural networks for function approximation? In *International Conference on Learning Representations (ICLR)*, 2016.
- Z. Liao, V. Quéto, V.-T. Nguyen, and E. Tartaglione. Can unstructured pruning reduce the depth in deep neural networks? In *Proceedings of the IEEE/CVF International Conference on Computer Vision (ICCV) Workshops*, 2023.
- Z. Liao, V. Qu'etu, V.-T. Nguyen, and E. Tartaglione. Nepenthe: Entropy-based pruning as a neural network depth's reducer. In *Arxiv*, 2024.
- S. Lohit and M. Jones. Model compression using optimal transport. *2022 IEEE/CVF Winter Conference on Applications of Computer Vision (WACV)*, 2020.
- S. Maji, J. Kannala, E. Rahtu, M. Blaschko, and A. Vedaldi. Fine-grained visual classification of aircraft, 2013.
- X. Men, M. Xu, Q. Zhang, B. Wang, H. Lin, Y. Lu, X. Han, and W. Chen. Shortgpt: Layers in large language models are more redundant than you expect, 2024.
- K. Nadjahi, A. Durmus, L. Chizat, S. Kolouri, S. Shahrampour, and U. Simsekli. Statistical and topological properties of sliced probability divergences. *Advances in Neural Information Processing Systems (NeurIPS)*, 2020.
- K. Nadjahi, A. Durmus, P. Jacob, R. Badeau, and U. Simsekli. Fast approximation of the sliced-wasserstein distance using concentration of random projections. In *Advances in Neural Information Processing Systems (NeurIPS)*, 2021.

- K. Nguyen and N. Ho. Amortized projection optimization for sliced wasserstein generative models. In *Advances in Neural Information Processing Systems (NeurIPS)*, 2022.
- V. Nguyen, T. Le, M. Yamada, and M. Osborne. Optimal transport kernels for sequential and parallel neural architecture search. In *International Conference on Machine Learning (ICML)*, 2020.
- M.-E. Nilsback and A. Zisserman. Automated flower classification over a large number of classes. In *Indian Conference on Computer Vision, Graphics and Image Processing*, Dec 2008.
- G. Peyré and M. Cuturi. Computational Optimal Transport. *Foundations and Trends in Machine Learning*, pages 355–206, 2018.
- V. Quétu and E. Tartaglione. Dsd²: Can we dodge sparse double descent and compress the neural network worry-free? In *AAAI*, 2024.
- V. Quétu, Z. Liao, and E. Tartaglione. The simpler the better: An entropy-based importance metric to reduce neural networks’ depth, 2024.
- J. Rabin and G. Peyré. Wasserstein regularization of imaging problem. In *2011 18th IEEE International Conference on Image Processing (ICIP)*, 2011.
- S. Santurkar, D. Tsipras, A. Ilyas, and A. Madry. How does batch normalization help optimization? In *Advances in Neural Information Processing Systems (NeurIPS)*, 2018.
- N. Si, J. Blanchet, S. Ghosh, and M. Squillante. Quantifying the empirical wasserstein distance to a set of measures: Beating the curse of dimensionality. In *Advances in Neural Information Processing Systems (NeurIPS)*, 2020.
- E. Tanguy, R. Flamary, and J. Delon. Properties of discrete sliced Wasserstein losses. *arXiv preprint*, 2023.
- E. Tartaglione, A. Bragagnolo, A. Fiandrotti, and M. Grangetto. Loss-based sensitivity regularization: Towards deep sparse neural networks. *Neural Networks*, 2022.
- T. Vayer and R. Gribonval. Controlling wasserstein distances by kernel norms with application to compressive statistical learning. *Journal of Machine Learning Research (JMLR)*, 2021.
- C. Villani. *Optimal transport : old and new*. Springer, 2009.
- J. Wu, Z. Huang, D. Acharya, W. Li, J. Thoma, D. P. Paudel, and L. V. Gool. Sliced wasserstein generative models. *2019 IEEE/CVF Conference on Computer Vision and Pattern Recognition (CVPR)*, 2019.
- J. Yang, Y. Liu, and H. Xu. Hotnas: Hierarchical optimal transport for neural architecture search. In *2023 IEEE/CVF Conference on Computer Vision and Pattern Recognition (CVPR)*, 2023.
- Y. Yang, Z. Cao, and H. Zhao. Laco: Large language model pruning via layer collapse. *ArXiv*, 2024.
- W. Zellinger, T. Grubinger, E. D. Lughofer, T. Natschläger, and S. Saminger-Platz. Central moment discrepancy (cmd) for domain-invariant representation learning, 2017.
- Z. Zhu, T. DING, J. Zhou, X. Li, C. You, J. Sulam, and Q. Qu. A geometric analysis of neural collapse with unconstrained features. In *Advances in Neural Information Processing Systems (NeurIPS)*, 2021.

A Broader Impact

We highlight the positive environmental impact of our work as it helps alleviate the high computational burden of neural networks, also allowing their deployment on resource-constrained devices.

B Gradients of the regularizer

Herein, we provide further details on the regularizer, namely, by deriving its gradients.

Namely, $\forall k_0 \in \llbracket K \rrbracket$,

$$\mathcal{R}_{k_0} = \sqrt{\frac{1}{N} \sum_{i=1}^N (\theta^T \mathbf{x}_{k_0,i} - \theta^T T_{k_0}(\mathbf{x}_{k_0,i}; w_{k_0}))^2} \quad (12)$$

In our setting, we are also assuming that $T_{k_0}(\mathbf{x}_{k_0,i}; w_{k_0}) = \mathbf{x}_{k_0,i} + f_{k_0}(\mathbf{x}_{k_0,i}; w_{k_0})$. Hence, we make use of this expression to derive the following analytical expression for $\frac{\partial \mathcal{R}_{k_0}}{\partial w_{k_0}}$.

$$\frac{\partial \mathcal{R}_{k_0}}{\partial w_{k_0}} = \frac{1}{N \mathcal{R}_{k_0}} \sum_{i=1}^N (\theta^T f_{k_0}(\mathbf{x}_{k_0,i}; w_{k_0})) \frac{\partial \theta^T f_{k_0}(\mathbf{x}_{k_0,i}; w_{k_0})}{\partial w_{k_0}} \quad (13)$$

$$\Rightarrow \frac{\partial \mathcal{R}}{\partial w_{k_0}} = \frac{1}{K} \sum_{k=k_0}^K \frac{\partial \mathcal{R}_k}{\partial w_{k_0}} \quad (14)$$

C Details on the learning strategies employed

The training hyperparameters used in the experiments are presented in Table 2. Our code is attached to this supplementary material and will be publicly available upon acceptance of the article.

CIFAR-10 is augmented with per-channel normalization, random horizontal flipping, and random shifting by up to four pixels in any direction. For the datasets of DomainBed, the images are augmented with per-channel normalization, random horizontal flipping, random cropping, and resizing to 224. The brightness, contrast, saturation, and hue are also randomly affected with a factor fixed to 0.4. Tiny-ImageNet-200 is augmented with per-channel normalization and random horizontal flipping. Moreover, the images of Flowers-102 are augmented with per-channel normalization, random horizontal and vertical flipping combined with a random rotation, and cropped to 224. DTD and Aircraft are augmented with random horizontal and vertical flipping, and with per-channel normalization.

Following Liao et al. [2023] and Quéту and Tartaglione [2024], on CIFAR-10 and Tiny-ImageNet-200, all the models are trained for 160 epochs, optimized with SGD, having momentum 0.9, batch size 128, and weight decay 1e-4. The learning rate is decayed by a factor of 0.1 at milestones 80 and 120. The initial learning rate ranges from 0.1 for ResNet-18 and MobileNetv2, 0.01 for VGG-16 to 1e-3 for Swin-T. Moreover, on PACS and VLCS, all the models are trained for 30 epochs, optimized with SGD, having momentum 0.9, a learning rate of 1e-3 decayed by a factor 0.1 at milestone 24, batch size 16, and weight decay 5e-4. Furthermore, on Aircraft, DTD, and Flowers-102, all the models are trained following a transfer learning strategy. Indeed, each model is initialized with their pre-trained weights on ImageNet, trained for 50 epochs, optimized with Adam, having a learning rate 1e-4 and batch size 16.

The experiments were mostly performed using an NVIDIA RTX 3090.

D Comparison with existing approaches

In this section, we compare our approach LaCoOT with the existing approaches: Iterative Magnitude Pruning (IMP) Han et al. [2015b], Layer Folding (LF) Dror et al. [2021], Entropy-Guided Pruning (EGP) Liao et al. [2023], NEPENTHE Liao et al. [2024], and EASIER Quéту et al. [2024]. Results on ResNet-18 trained on CIFAR-10 are presented in Table 3.

As expected, after 7 iterations, IMP is not able to remove any layers from the architecture, although it maintains the performance of the original model. Concerning LF, the method already affects performance after removing one layer. On the other hand, EGP, NEPENTHE and EASIER methods enable multiple layers deletion while maintaining

Model	Dataset	Epochs	Batch	Opt.	Mom.	LR	Milestones	Drop Factor	Weight Decay
ResNet-18	CIFAR-10	160	128	SGD	0.9	0.1	[80, 120]	0.1	1e-4
Swin-T	CIFAR-10	160	128	SGD	0.9	0.001	[80, 120]	0.1	1e-4
MobileNetv2	CIFAR-10	160	128	SGD	0.9	0.1	[80, 120]	0.1	1e-4
VGG-16	CIFAR-10	160	128	SGD	0.9	0.01	[80, 120]	0.1	1e-4
ResNet-18	Tiny-ImageNet-200	160	128	SGD	0.9	0.1	[80, 120]	0.1	1e-4
Swin-T	Tiny-ImageNet-200	160	128	SGD	0.9	0.001	[80, 120]	0.1	1e-4
MobileNetv2	Tiny-ImageNet-200	160	128	SGD	0.9	0.1	[80, 120]	0.1	1e-4
VGG-16	Tiny-ImageNet-200	160	128	SGD	0.9	0.01	[80, 120]	0.1	1e-4
ResNet-18	PACS	30	16	SGD	0.9	0.001	[24]	0.1	5e-4
Swin-T	PACS	30	16	SGD	0.9	0.001	[24]	0.1	5e-4
MobileNetv2	PACS	30	16	SGD	0.9	0.001	[24]	0.1	5e-4
VGG-16	PACS	30	16	SGD	0.9	0.001	[24]	0.1	5e-4
ResNet-18	VLCS	30	16	SGD	0.9	0.001	[24]	0.1	5e-4
Swin-T	VLCS	30	16	SGD	0.9	0.001	[24]	0.1	5e-4
MobileNetv2	VLCS	30	16	SGD	0.9	0.001	[24]	0.1	5e-4
VGG-16	VLCS	30	16	SGD	0.9	0.001	[24]	0.1	5e-4
ResNet-18	Flowers-102	50	16	Adam		1e-4			0
Swin-T	Flowers-102	50	16	Adam		1e-4			0
MobileNetv2	Flowers-102	50	16	Adam		1e-4			0
VGG-16	Flowers-102	50	16	Adam		1e-4			0
ResNet-18	DTD	50	16	Adam		1e-4			0
Swin-T	DTD	50	16	Adam		1e-4			0
MobileNetv2	DTD	50	16	Adam		1e-4			0
VGG-16	DTD	50	16	Adam		1e-4			0
ResNet-18	Aircraft	50	16	Adam		1e-4			0
Swin-T	Aircraft	50	16	Adam		1e-4			0
MobileNetv2	Aircraft	50	16	Adam		1e-4			0
VGG-16	Aircraft	50	16	Adam		1e-4			0

Table 2: The different employed learning strategies.

Dataset	Approach	ResNet-18	
		top-1 [%]	Rem.
CIFAR-10	Original	91,77	0
	IMP	91,66	0
	LF	90,65	1
	EGP	92,00	3
	NEPENTHE	92,55	3
	EASIER	92,10	8
	LaCoOT ($\lambda = 0$)	64,46	16
	LaCoOT (λ_{LOW})	89,01	16
	LaCoOT (λ_{HIGH})	90,99	16

Table 3: Test performance (top-1) and number of removed layers (Rem.) of ResNet-18 trained with different methods on CIFAR-10.

performance, respectively 3, 3, and 8. Nevertheless, LaCoOT achieves the best compromise between performance and complexity and demonstrates its effectiveness by being able to remove 16 layers with a slight sacrifice in performance. Unlike its competitors, LaCoOT produces compressed models in a single training, without requiring any fine-tuning after removing layers which clearly demonstrates its superiority.

E Detailed results

For all the datasets, the test performance (top-1) and the number of multiply-accumulate operations (MACs) obtained by LaCoOT with different λ are displayed in Table 4 for ResNet-18, in Table 5 for Swin-T, and in Table 6 for MobileNetv2.

Dataset	Rem.	LaCoOT($\lambda = 0$)		LaCoOT($\lambda = 0, 01$)		LaCoOT($\lambda = 0, 1$)		LaCoOT($\lambda = 1$)		LaCoOT($\lambda = 5$)	
		top-1[%]	MACs(\downarrow)	top-1[%]	MACs(\downarrow)	top-1[%]	MACs(\downarrow)	top-1[%]	MACs(\downarrow)	top-1[%]	MACs(\downarrow)
CIFAR-10	0	91,77	140,19 M	91,53	140,19 M	91,76	140,19 M	91,38	140,19 M	90,93	140,19 M
	1	91,68	121,31 M	91,56	121,31 M	91,69	121,31 M	91,39	121,31 M	90,93	121,31 M
	2	79,93	102,44 M	90,33	102,44 M	91,07	102,44 M	91,37	102,44 M	90,93	102,44 M
	3	77,63	83,56 M	80,66	83,56 M	84,13	83,56 M	91,31	83,56 M	90,95	83,56 M
	4	64,46	64,69 M	73,04	64,69 M	80,23	64,69 M	89,01	64,69 M	90,99	64,69 M
Tiny ImageNet 200	0	41,48	148,15 M	–	–	–	–	40,84	148,15 M	39,52	148,15 M
	1	39,40	129,27 M	–	–	–	–	40,84	129,27 M	39,52	129,27 M
	2	36,66	110,4 M	–	–	–	–	40,80	110,40 M	39,54	110,40 M
	3	31,56	91,53 M	–	–	–	–	40,18	91,53 M	38,62	91,53 M
	4	29,14	72,65 M	–	–	–	–	37,32	72,65 M	38,02	72,65 M
PACS	0	79,10	6,87 G	79,90	6,87 G	80,40	6,87 G	74,60	6,87 G	48,70	6,87 G
	1	52,00	5,94 G	30,00	5,94 G	57,30	5,94 G	70,80	5,94 G	50,20	5,94 G
	2	31,50	5,02 G	26,80	5,02 G	39,20	5,02 G	63,80	5,02 G	49,30	5,02 G
	3	17,70	4,09 G	24,70	4,09 G	24,60	4,09 G	53,20	4,09 G	47,60	4,09 G
	4	15,10	3,17 G	15,20	3,17 G	16,90	3,17 G	39,30	3,17 G	47,80	3,17 G
VLCS	0	69,06	6,87 G	68,03	6,87 G	67,47	6,87 G	63,47	6,87 G	53,77	6,87 G
	1	55,55	5,94 G	53,49	5,94 G	56,38	5,94 G	60,76	5,94 G	52,19	5,94 G
	2	49,02	5,02 G	48,37	5,02 G	51,35	5,02 G	60,58	5,02 G	53,22	5,02 G
	3	48,18	4,09 G	44,27	4,09 G	46,32	4,09 G	56,57	4,09 G	53,31	4,09 G
	4	41,10	3,17 G	42,87	3,17 G	45,67	3,17 G	53,12	3,17 G	53,12	3,17 G
Flowers 102	0	89,32	1,81 G	89,45	1,81 G	89,35	1,81 G	87,97	1,81 G	60,90	1,81 G
	1	82,81	1,58 G	82,19	1,58 G	83,28	1,58 G	82,44	1,58 G	56,38	1,58 G
	2	51,08	1,35 G	51,15	1,35 G	52,89	1,35 G	62,14	1,35 G	44,66	1,35 G
	3	8,94	1,12 G	8,29	1,12 G	9,79	1,12 G	20,56	1,12 G	31,26	1,12 G
	4	5,94	888,77 M	4,57	888,77 M	5,04	888,77 M	10,94	888,77 M	18,80	888,77 M
DTD	0	61,38	1,81 G	59,95	1,81 G	60,48	1,81 G	60,37	1,81 G	57,82	1,81 G
	1	55,43	1,58 G	53,94	1,58 G	54,31	1,58 G	57,18	1,58 G	55,43	1,58 G
	2	35,43	1,35 G	32,82	1,35 G	34,89	1,35 G	43,94	1,35 G	45,48	1,35 G
	3	13,51	1,12 G	12,23	1,12 G	16,28	1,12 G	23,51	1,12 G	33,56	1,12 G
	4	6,12	888,74 M	6,54	888,74 M	7,18	888,74 M	14,26	888,74 M	31,49	888,74 M
Aircraft	0	74,32	1,81 G	73,30	1,81 G	74,02	1,81 G	73,39	1,81 G	54,73	1,81 G
	1	61,33	1,58 G	57,82	1,58 G	59,83	1,58 G	62,98	1,58 G	48,18	1,58 G
	2	27,00	1,35 G	27,06	1,35 G	31,62	1,35 G	41,07	1,35 G	39,60	1,35 G
	3	4,53	1,12 G	5,97	1,12 G	7,50	1,12 G	20,82	1,12 G	31,92	1,12 G
	4	3,03	888,77 M	2,49	888,77 M	3,57	888,77 M	8,82	888,77 M	24,99	888,77 M

Table 4: Test performance (top-1) and number of multi-accumulate operations (MACs) depending on the number of removed blocks (Rem.) of ResNet-18 trained with LaCoOT with different λ on all the considered setups. 0 refers to the original model without layer deletion.

Dataset	Rem.	LaCoOT($\lambda = 0$)		LaCoOT($\lambda = 0, 001$)		LaCoOT($\lambda = 0, 01$)		LaCoOT($\lambda = 0, 1$)		LaCoOT($\lambda = 1$)	
		top-1[%]	MACs(\downarrow)	top-1[%]	MACs(\downarrow)	top-1[%]	MACs(\downarrow)	top-1[%]	MACs(\downarrow)	top-1[%]	MACs(\downarrow)
CIFAR-10	0	91.67	518,94 M	91.70	518,94 M	91.50	518,94 M	91.38	518,94 M	90.72	518,94 M
	1	88.91	505,08 M	88.73	505,08 M	88.74	505,08 M	88.69	505,08 M	86.47	505,08 M
	2	79.15	492,17 M	78.78	492,17 M	78.85	492,17 M	83.24	492,17 M	81.48	492,17 M
	3	45.28	479,27 M	45.23	479,27 M	44.83	479,27 M	47.40	479,27 M	72.26	456,64 M
	4	26.25	443,73 M	26.07	443,73 M	26.52	443,73 M	47.32	443,73 M	37.92	442,77 M
	5	26.25	443,73 M	26.07	443,73 M	26.52	443,73 M	47.24	319,57 M	32.19	407,23 M
	6	12.61	429,87 M	12.47	429,87 M	20.31	408,19 M	28.64	284,03 M	18.03	394,33 M
7	16.59	394,33 M	16.22	394,33 M	16.90	394,33 M	27.73	248,49 M	11.49	358,79 M	
Tiny ImageNet 200	0	75.48	772,45 M	75.64	772,45 M	75.56	772,45 M	75.18	772,45 M	72.36	772,45 M
	1	72.74	720,83 M	72.76	720,83 M	72.92	720,83 M	71.70	733,0 M	69.78	733,0 M
	2	66.90	681,38 M	66.70	681,38 M	66.36	681,38 M	66.28	681,38 M	64.46	681,38 M
	3	23.00	629,77 M	24.30	629,77 M	57.28	631,69 M	26.94	629,77 M	15.52	641,93 M
	4	6,70	580,08 M	7,00	580,08 M	6,96	580,08 M	8,86	580,08 M	15,52	641,93 M
	5	1,68	530,38 M	1,09	530,38 M	1,94	530,38 M	8,86	580,08 M	2,82	590,32 M
	6	1,50	480,69 M	1,96	480,69 M	1,70	480,69 M	2,38	530,38 M	2,06	540,63 M
7	0,94	430,99 M	1,14	430,99 M	0,98	430,99 M	0,80	490,93 M	1,30	490,93 M	
PACS	0	97.00	4,5 G	96.90	4,5 G	96.90	4,5 G	97.10	4,5 G	96.00	4,5 G
	1	95.40	4,12 G	95.50	4,12 G	95.10	4,13 G	96.20	4,12 G	95.80	4,12 G
	2	91.70	3,76 G	93.10	3,76 G	91.80	3,76 G	93.20	3,76 G	93.70	3,76 G
	3	83.40	3,4 G	80.70	3,4 G	39.80	3,39 G	48.20	3,39 G	56.80	3,38 G
	4	17.40	3,04 G	19.03	3,04 G	21.00	3,04 G	14.60	3,02 G	18.90	3,02 G
	5	14.80	2,68 G	15.07	2,68 G	17.20	2,68 G	14.90	3,02 G	18.20	2,66 G
	6	13.50	2,68 G	16.60	2,68 G	16.70	2,68 G	14.00	2,66 G	16.04	2,66 G
7	16.60	2,31 G	15.70	2,31 G	15.80	2,33 G	14.20	2,31 G	16.50	2,31 G	
VLCS	0	83.04	4,5 G	83.60	4,5 G	83.13	4,5 G	83.88	4,5 G	83.88	4,5 G
	1	82.67	4,13 G	82.11	4,13 G	82.48	4,13 G	82.48	4,13 G	82.20	4,12 G
	2	81.08	3,76 G	81.45	3,78 G	80.24	3,76 G	80.80	3,76 G	81.64	3,76 G
	3	76.42	3,4 G	76.23	3,4 G	76.98	3,4 G	77.07	3,4 G	53.68	3,38 G
	4	39.79	3,04 G	12.58	3,04 G	28.70	3,04 G	30.10	3,04 G	51.63	3,02 G
	5	35.23	2,68 G	38.58	2,68 G	44.36	2,68 G	44.92	2,68 G	17.43	2,66 G
	6	37.65	2,68 G	38.40	2,68 G	44.08	2,68 G	43.90	2,68 G	12.12	2,31 G
7	41.57	2,33 G	43.52	2,33 G	44.83	2,33 G	44.73	2,33 G	11.65	2,31 G	
Flowers 102	0	92.19	4,5 G	92.21	4,5 G	91.90	4,5 G	92.08	4,5 G	91.92	4,5 G
	1	90.89	4,13 G	91.12	4,13 G	91.07	4,13 G	90.93	4,13 G	90.08	4,13 G
	2	86.10	3,76 G	85.56	3,76 G	85.53	3,76 G	85.49	3,76 G	84.26	3,76 G
	3	44.23	3,39 G	45.00	3,39 G	46.09	3,39 G	42.64	3,39 G	50.04	3,39 G
	4	25.66	3,04 G	45.00	3,39 G	46.09	3,39 G	24.83	3,04 G	4.91	3,02 G
	5	25.66	3,04 G	7.68	3,02 G	26.17	3,04 G	24.83	3,04 G	4.10	2,66 G
	6	5.98	2,66 G	6.36	2,66 G	6.39	2,66 G	5.69	2,66 G	4.10	2,66 G
7	3.43	2,31 G	4.42	2,31 G	3.97	2,31 G	5.04	2,31 G	4.23	2,31 G	
DTD	0	68.51	4,5 G	68.83	4,5 G	67.71	4,5 G	67.77	4,5 G	66.01	4,5 G
	1	65.37	4,12 G	66.97	4,13 G	64.84	4,12 G	65.00	4,12 G	64.31	4,12 G
	2	60.43	3,76 G	61.70	3,76 G	53.67	3,76 G	53.24	3,76 G	58.72	3,76 G
	3	24.68	3,39 G	26.81	3,39 G	23.19	3,39 G	24.36	3,39 G	25.69	3,39 G
	4	11.76	3,04 G	12.18	3,04 G	11.86	3,04 G	6.97	3,02 G	4.15	3,02 G
	5	11.76	3,04 G	4.57	2,66 G	3.78	2,66 G	3.40	2,66 G	4.15	3,02 G
	6	4.52	2,66 G	4.57	2,66 G	3.78	2,66 G	3.40	2,66 G	2.98	2,66 G
7	3.19	2,31 G	2.66	2,31 G	2.55	2,31 G	2.23	2,31 G	2.98	2,31 G	
Aircraft	0	78.16	4,5 G	76.09	4,5 G	75.43	4,5 G	75.91	4,5 G	77.08	4,5 G
	1	74.35	4,12 G	73.00	4,12 G	71.50	4,12 G	70.90	4,12 G	74.17	4,12 G
	2	66.97	3,76 G	64.69	3,76 G	61.69	3,76 G	60.13	3,76 G	66.49	3,76 G
	3	66.97	3,76 G	18.75	3,39 G	10.92	3,39 G	12.66	3,39 G	66.49	3,76 G
	4	20.46	3,38 G	2.40	3,02 G	1.68	3,02 G	2.10	3,02 G	16.50	3,38 G
	5	2.31	3,02 G	2.40	3,02 G	1.68	3,02 G	2.10	3,02 G	1.41	3,02 G
	6	0.87	2,66 G	1.29	2,66 G	1.23	2,66 G	1.53	2,66 G	0.87	2,66 G
7	0.96	2,31 G	1.20	2,31 G	1.08	2,31 G	0.87	2,31 G	1.20	2,31 G	

Table 5: Test performance (top-1) and number of multi-accumulate operations (MACs) depending on the number of removed blocks (Rem.) of Swin-T trained with LaCoOT with different λ on all the considered setups. 0 refers to the original model without layer deletion.

Dataset	Rem.	LaCoOT($\lambda = 0$)		LaCoOT($\lambda = 0, 001$)		LaCoOT($\lambda = 0, 01$)		LaCoOT($\lambda = 0, 1$)		LaCoOT($\lambda = 1$)	
		top-1[%]	MMACs(\downarrow)	top-1[%]	MMACs(\downarrow)	top-1[%]	MMACs(\downarrow)	top-1[%]	MMACs(\downarrow)	top-1[%]	MMACs(\downarrow)
CIFAR-10	0	93,50	87,98	93,31	87,98	93,31	87,98	93,47	87,98	91,86	87,98
	1	90,01	87,84	89,11	87,84	90,96	87,84	91,51	87,64	88,46	87,53
	2	81,41	87,51	82,41	87,51	85,56	87,51	87,91	87,51	87,85	87,2
	3	66,28	87,17	66,23	87,17	74,0	87,17	84,64	87,29	84,87	86,98
	4	9,47	86,95	17,44	86,95	12,18	86,95	13,72	87,06	15,65	86,76
	5	9,43	86,73	11,4	86,82	11,29	86,73	14,17	86,84	16,58	86,62
	6	10,97	86,51	9,52	86,59	8,73	86,51	14,0	86,4	12,19	85,29
	7	11,09	86,37	8,99	86,37	6,87	86,37	16,34	86,07	11,72	84,41
Tiny ImageNet 200	0	45,92	24,7	44,98	24,7	46,74	24,7	45,90	24,7	43,88	24,7
	1	40,84	24,62	40,14	24,62	41,92	24,62	41,98	24,65	40,68	24,59
	2	32,72	24,59	31,72	24,59	33,2	24,59	41,1	24,59	40,68	24,48
	3	30,46	24,53	28,06	24,53	0,42	24,53	37,78	24,51	40,68	24,43
	4	24,92	24,45	22,1	24,48	0,6	24,48	31,1	24,48	40,68	24,37
	5	0,58	24,39	17,46	24,39	0,68	24,42	0,46	24,42	3,98	24,32
	6	0,8	24,34	0,88	24,34	0,88	24,34	0,52	24,34	3,98	24,23
	7	0,94	24,23	0,66	24,23	0,68	24,23	0,56	24,23	2,88	23,9
PACS	0	95,40	299,51	95,00	299,51	95,50	299,51	95,70	299,51	95,70	299,51
	1	85,6	298,83	91,1	298,83	77,2	298,83	84,8	298,83	92,4	298,83
	2	50,7	297,81	56,7	297,81	50,2	297,81	61,7	298,15	84,9	297,47
	3	12,0	297,13	14,2	297,13	17,9	297,13	13,3	297,47	67,5	296,79
	4	11,9	296,46	12,4	296,46	17,5	296,46	14,6	296,46	19,0	296,12
	5	10,6	295,44	6,8	295,44	18,8	295,44	12,0	295,44	16,7	292,05
	6	9,8	295,02	9,6	295,02	9,9	295,02	16,6	294,08	17,1	290,7
	7	9,08	293,66	9,7	293,66	9,8	293,66	11,0	293,66	17,8	290,7
VLCS	0	80,90	299,51	79,40	299,51	81,27	299,51	79,40	299,51	79,87	299,51
	1	57,04	298,82	60,95	298,82	74,00	298,82	66,45	298,82	79,22	298,82
	2	42,78	298,15	56,38	297,81	54,80	297,81	53,87	298,15	65,33	298,15
	3	43,34	297,13	21,90	297,13	34,67	297,13	46,60	297,13	51,91	296,79
	4	5,96	296,45	35,32	296,45	16,22	296,45	23,86	296,45	6,99	296,11
	5	9,88	295,1	45,85	295,44	22,93	295,1	35,60	296,03	9,41	294,76
	6	27,87	294,08	45,85	294,08	26,84	294,08	26,65	295,01	20,41	290,69
	7	24,14	293,66	26,84	293,66	27,21	293,66	29,73	293,66	12,49	289,68
Flowers 102	0	91,10	299,51	90,84	299,51	90,84	299,51	90,55	299,51	90,83	299,51
	1	51,46	298,95	80,86	298,95	81,17	298,95	57,03	298,95	84,32	298,95
	2	31,84	298,27	31,91	298,27	31,24	298,27	2,72	298,27	48,66	298,27
	3	1,84	297,59	2,23	297,59	26,04	297,25	2,24	297,59	4,73	297,59
	4	0,85	296,58	1,50	296,58	20,30	296,24	1,33	296,58	1,82	296,58
	5	1,40	295,56	1,19	296,15	1,32	295,56	1,27	295,56	1,35	295,56
	6	1,15	295,14	0,89	295,14	1,68	295,14	2,42	295,14	1,95	294,21
	7	0,81	293,78	0,83	293,78	1,25	293,78	2,46	293,78	4,44	293,78
DTD	0	63,94	299,51	64,04	299,51	63,67	299,51	63,56	299,51	64,31	299,51
	1	53,24	298,88	53,03	298,88	52,77	298,88	5,11	298,88	56,33	298,88
	2	16,60	298,2	4,47	298,2	17,66	298,2	5,00	298,2	6,33	298,2
	3	3,67	297,52	3,62	297,52	3,88	297,52	4,20	297,52	5,21	297,52
	4	2,45	296,51	2,34	296,51	2,23	296,51	2,34	296,51	2,93	296,51
	5	2,87	295,49	2,98	295,49	2,61	295,49	2,45	295,49	3,03	295,15
	6	2,87	294,14	3,03	294,14	1,91	294,14	2,45	294,14	4,04	294,14
	7	3,78	293,71	2,98	293,71	2,93	293,71	2,82	293,71	2,66	292,78
Aircraft	0	74,38	299,51	74,17	299,51	74,62	299,51	74,62	299,51	73,51	299,51
	1	46,44	298,94	49,32	298,94	59,68	298,94	51,25	298,94	64,00	298,94
	2	37,32	298,27	37,14	298,27	38,61	298,27	37,50	298,27	51,01	298,27
	3	1,59	297,59	1,65	297,59	1,14	297,59	1,56	297,59	17,67	296,91
	4	1,11	296,57	1,08	296,57	1,08	296,24	1,59	296,57	1,47	296,24
	5	0,84	295,22	1,41	295,56	1,17	295,22	1,14	295,56	1,50	295,22
	6	0,90	294,2	1,20	294,2	1,17	294,2	1,17	294,2	1,62	293,86
	7	0,99	293,78	1,38	293,78	1,20	293,78	1,56	292,85	1,35	292,85

Table 6: Test performance (top-1) and number of multi-accumulate operations (MACs) depending on the number of removed blocks (Rem.) of MobileNetv2 trained with LaCoOT with different λ on all the considered setups. 0 refers to the original model without layer deletion.